

SPECTRALLY RESOLVED LOCAL CELLO CHARACTERIZATION OF TANDEM SOLAR CELLS USING LINEAR AND 2ND HARMONIC RESPONSE ANALYSIS

A. Schütt^{a)}, J. Carstensen^{a)}, J.-M. Wagner^{a)}, H. Föll^{a)},
M. Nguyen^{b)}, and S. Klein^{b)}

^{a)}: Institute for General Materials Science, Faculty of Engineering, Christian-Albrechts-University of Kiel,
Kaiserstr. 2, 24143 Kiel, Germany, email: jc@tf.uni-kiel.de, Phone: (+49) 431 880 6181, Fax: (+49) 431 880 6178

^{b)}: Robert Bosch GmbH, Corporate Research, Robert-Bosch-Platz 1, 70839 Gerlingen-Schillerhöhe

ABSTRACT: In this paper the CELLO technique (solar CELLOcal characterization) is used for the local characterization of a-Si/ μ -Si tandem solar cells. Applying a blue and an infrared laser in a confocal beam with different frequencies for the modulation of the intensities, the cells can be analyzed with respect to local current matching. Combining these data with e.g. the 2nd harmonic response, i.e. the local non-linear interaction of the short-circuit photocurrents generated by both lasers, additional local properties like the diode characteristics (leakage currents) of both sub-cells, or local series resistances can be analyzed. Several examples for the identification of local defects by combining CELLO maps will be discussed.

Keywords: Characterization, a-Si/ μ -Si, Current matching

1 INTRODUCTION

Since in multijunction solar cells several sub-cells are connected in series, current matching (CM) of all sub-cells is necessary for optimal performance, i.e. sub-cells in the (local) current path should generate the same amount of photocurrent. Without CM the sub-cell with the lowest photo current is limiting the (local) current of the device. For analyzing the photocurrent generated in individual sub-cells often the other sub-cells are "flooded" with charges by global illumination with light of certain wavelength selectively absorbed in these sub-cells.

The new method presented in this paper uses simultaneously generated photocurrent in both sub-cells and the characterization of their non-linear interaction via 2nd harmonic analysis that e.g. allows to study CM and other non-linear effects.

2 THEORY

For any photo current response of a solar cell on (local) illumination with intensity I , a possible modulation of the intensity with (angular) frequency $\omega = 2\pi f$ using light with a wavelength λ can be represented as a Taylor series

$$F(I, \omega, \lambda) = c_0(I_0, \omega, \lambda) + c_1(I_0, \omega, \lambda)(I - I_0) + c_2(I_0, \omega, \lambda)(I - I_0)^2 + \dots \quad (1)$$

Applying two periodically modulated signals to two lasers a and b with different wavelengths,

$$(I - I_0) = I_a \cos(\omega_a t) + I_b \cos(\omega_b t) \quad (2)$$

holds, which according to Eq. (1) leads to a linear response

$$c_1(I_0, \omega_a, \lambda_a) I_a \cos(\omega_a t) + c_1(I_0, \omega_b, \lambda_b) I_b \cos(\omega_b t). \quad (3)$$

The response in second order contains three components with different frequencies:

$$c_2(I_0, \omega_a, \lambda_a) I_a^2 \frac{\cos(2\omega_a t) + 1}{2}, \quad (4a)$$

$$c_2(I_0, \omega_b, \lambda_b) I_b^2 \frac{\cos(2\omega_b t) + 1}{2}, \quad (4b)$$

$$c_2(I_0, \omega_a, \lambda_a, \omega_b, \lambda_b) I_a I_b \times [\cos((\omega_a + \omega_b)t) + \cos((\omega_a - \omega_b)t)]. \quad (4c)$$

Typically, for analyzing the effect of Eq. (4c) only the response with the frequency $(\omega_a + \omega_b)$ is used and this technique related to Eqs. (4a–c) is called 2nd harmonic analysis.

Eqs. (4a) and (4b) denote non-linearities which are related to processes of only one of the two lasers alone. In contrast, Eq. (4c) reflects non-linear (local) interactions of charge carriers generated by both lasers in the solar cell, which is the main focus of this paper. In the CELLO measurements presented here two confocal sinusoidally intensity modulated laser beams act as perturbation, scanning across a solar cell while a fast potentiostat controls the cell potential to be 0 mV. A lock-in routine allows to extract amplitude maps ($A_{x,y}$) and phase shift maps ($\varphi_{x,y}$) for up to 8 frequencies simultaneously in one scan across the solar cell; in this paper the maps for ω_a , ω_b , $2\omega_a$, $2\omega_b$, and $(\omega_a + \omega_b)$ are discussed.

On multicrystalline Si solar cells the 2nd harmonic response has already been used to analyze non-linear effects [1] like those related to injection level dependencies or bad charge separation on p-n junctions of UMG solar cells in strongly compensated regions. For the tandem cell investigated here blue laser light (401 nm) is only absorbed in the a-Si top cell while IR light (830 nm) is mainly absorbed in the μ -Si bottom cell. Current matching in this cell structure means that photo current from the top cell and photo current from the bottom cell is needed to allow for a photo current flow through the tandem structure; this is an extreme form of non-linear interaction and thus can be analyzed locally using Eq. (4c). Modulating the IR laser with ω_a and the blue laser with ω_b current matching can be analyzed either directly by the amplitude map $A_{x,y}(\omega_a + \omega_b)$ and the phase shift map $\varphi_{x,y}(\omega_a + \omega_b)$ or by calculating the amplitude ratio

$$\frac{A_{x,y}(\omega_a + \omega_b)}{A_{x,y}(\omega_a)A_{x,y}(\omega_b)} = \left| \frac{c_2(I_0, \omega_a, \lambda_a, \omega_b, \lambda_b)}{c_2(I_0, \omega_a, \lambda_a)c_2(I_0, \omega_b, \lambda_b)} \right| \quad (5)$$

and the corresponding phase shift differences. The benefit of Eq. (5) is that local effects like differences in the spectrally dependent reflectivity and differences in the lateral ohmic losses cancel out.

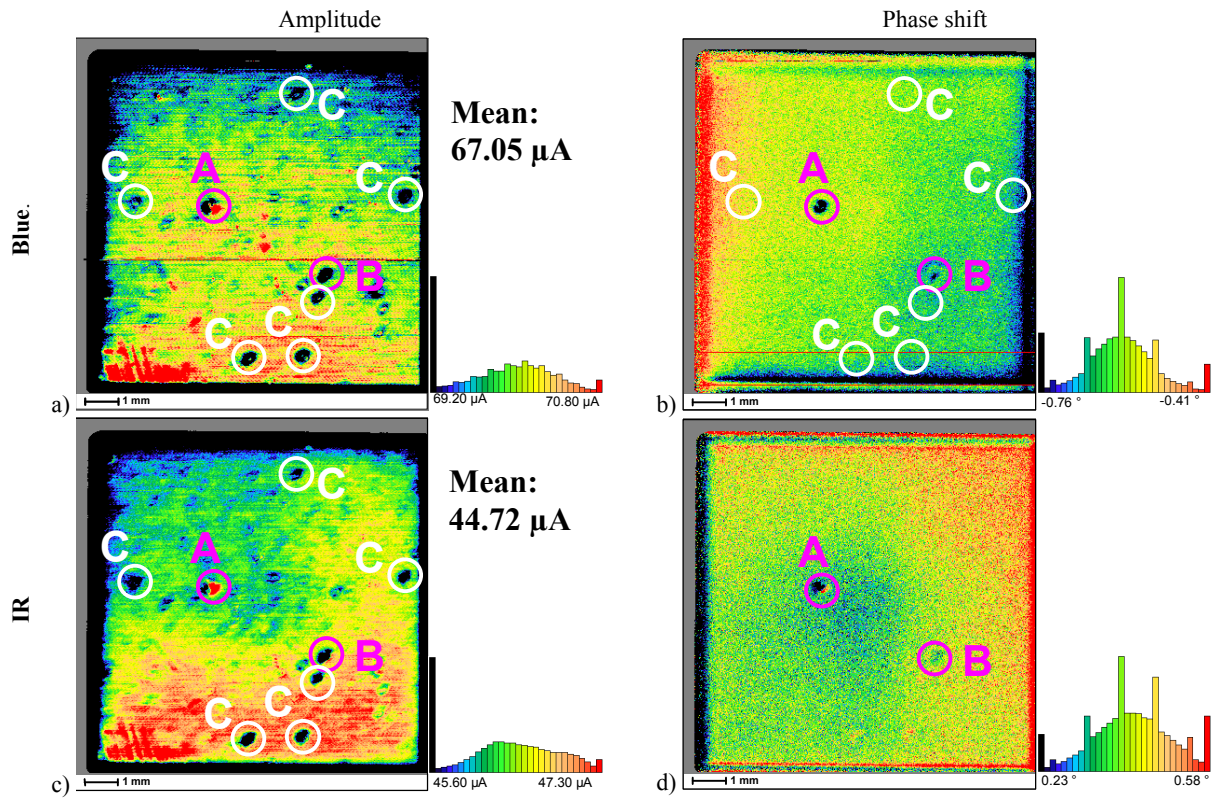


Fig. 1: a) Amplitude map $A_{x,y}(\omega_a)$ and b) phase shift map $\varphi_{x,y}(\omega_a)$ of the short-circuit current of the blue laser (at 6 kHz), measured with the confocal IR laser at full constant intensity. c) Amplitude map $A_{x,y}(\omega_a)$ and d) phase shift map $\varphi_{x,y}(\omega_a)$ of the short-circuit current of the IR laser (at 6 kHz), measured with the confocal blue laser at full constant intensity.

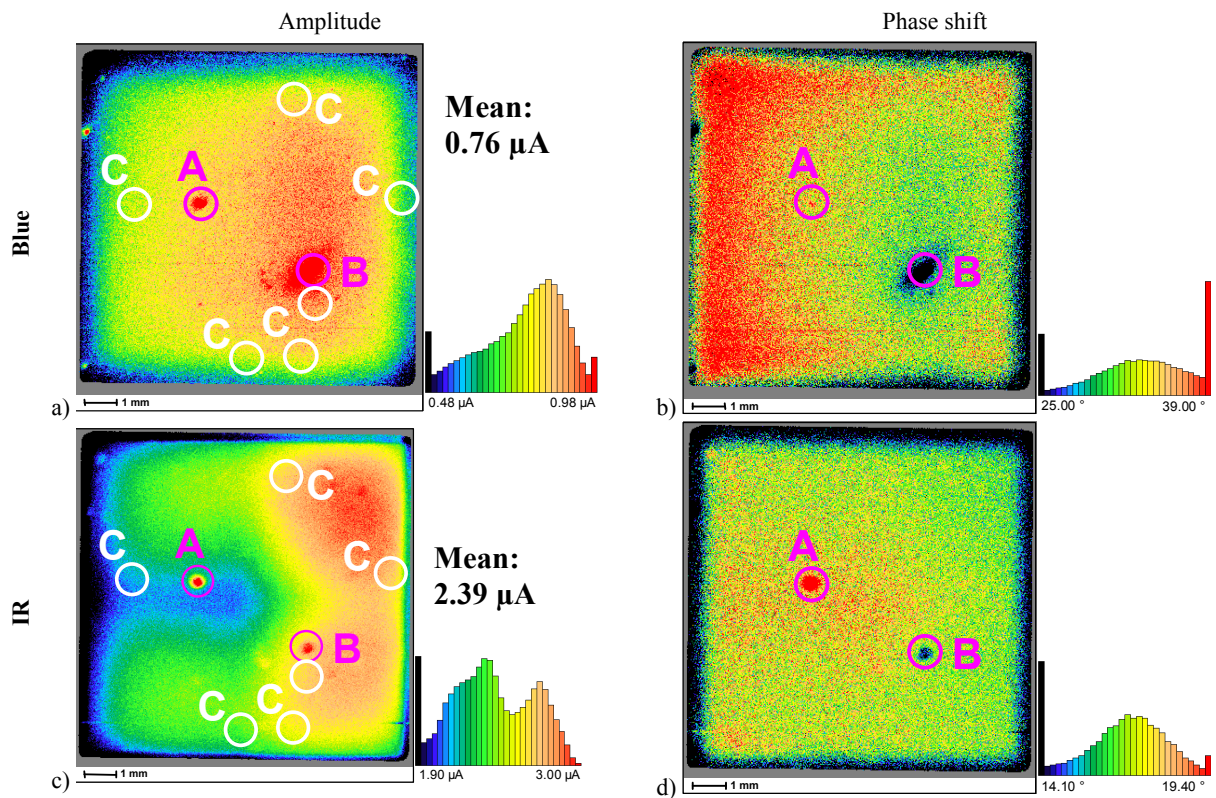


Fig. 2: a) Amplitude map $A_{x,y}(\omega_a)$ and b) phase shift map $\varphi_{x,y}(\omega_a)$ of the short-circuit current of the blue laser (at 6 kHz), measured while the IR laser is switched off. c) Amplitude map $A_{x,y}(\omega_a)$ and d) phase shift map $\varphi_{x,y}(\omega_a)$ of the short-circuit current of the IR laser (at 6 kHz), measured while the blue laser is switched off.

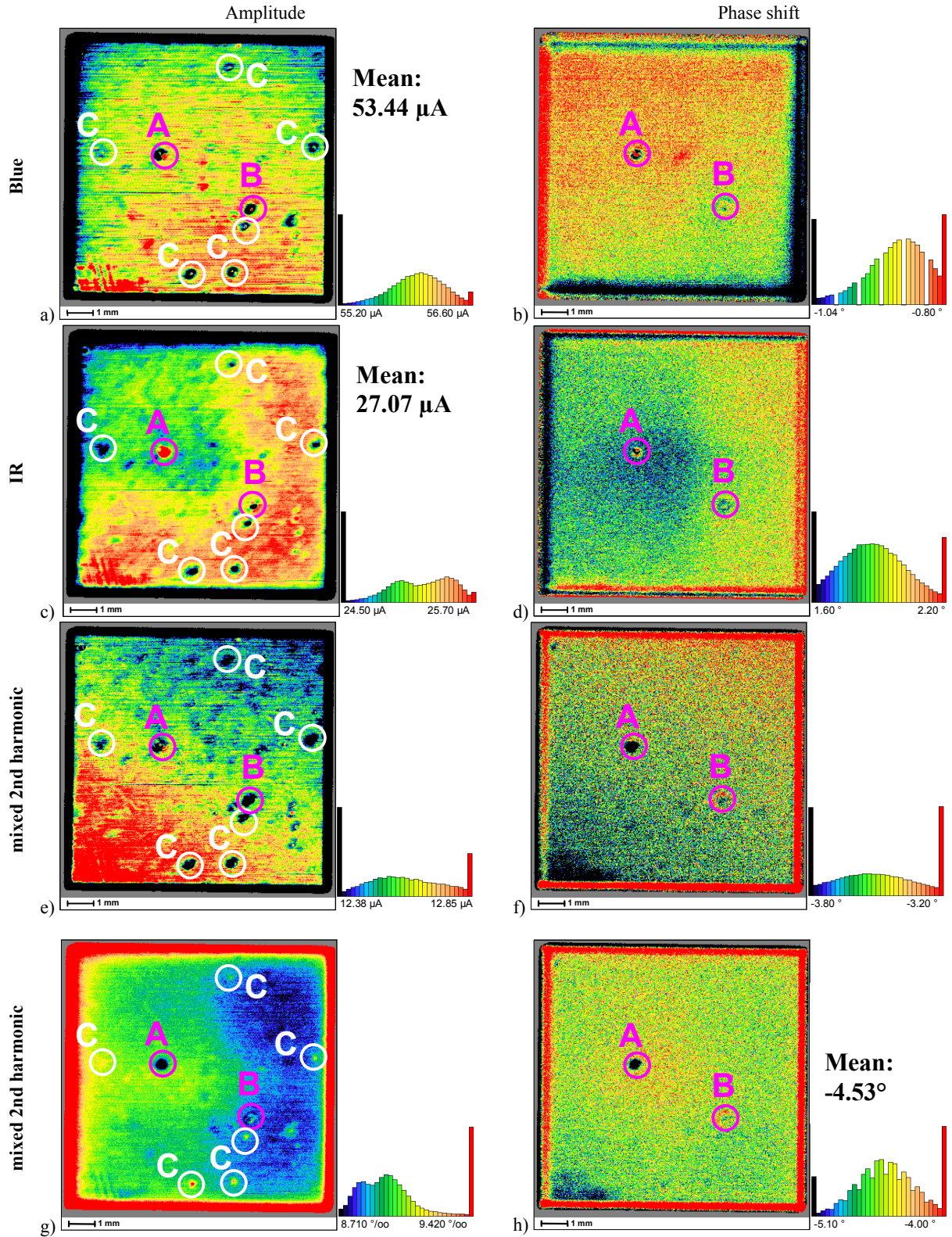


Fig. 3: Simultaneously measured short-circuit photocurrent maps using two confocal laser beams: blue laser at frequency $f_a = 10$ kHz, IR laser at frequency $f_b = 6$ kHz; a) amplitude map $A_{x,y}(\omega_a)$ and b) phase shift map $\varphi_{x,y}(\omega_a)$ of the blue laser; c) amplitude map $A_{x,y}(\omega_b)$ and d) phase shift map $\varphi_{x,y}(\omega_b)$ of the IR laser; e) amplitude map $A_{x,y}(\omega_a + \omega_b)$ and f) phase shift map $\varphi_{x,y}(\omega_a + \omega_b)$ of mixed 2nd harmonic between blue and IR laser photo current; g) amplitude ratio map according to Eq. (5), i.e. Fig. 3e) divided by Fig. 3a) and Fig. 3c), contains cell information equivalent to measurements in Fig. 2c); h) phase shift ratio map according to Eq. (5), i.e. Fig. 3f) minus Fig. 3b) and minus Fig. 3d).

3 EXPERIMENTAL

3.1 Sample

An a-Si/ μ -Si tandem solar cell test structure produced at the Bosch Corporate Research laboratory ($\eta = 10.5\%$, $FF = 73.3\%$, $U_{oc} = 1372$ mV, $J_{sc} = 10.45$ mA/cm²) is analyzed. The sample is a blue light sensitive a-Si top cell and an infrared light sensitive μ -Si bottom cell of 1 cm² area.

3.2 CELLO measurements

Three sets of experiments have been performed using combinations of two confocal laser beams (Blue 401 nm, IR 830 nm) in the standard CELLO setup [2].

In a first experiment set the blue (IR) laser is modulated with frequency $\omega_a = 2\pi \times 6$ kHz while the confocal IR (blue) laser works at full intensity, i.e. the non-modulated IR (blue) laser serves as background illumination, "flooding" the bottom (top) cell with charge carriers and thus allowing for a "standard" LBIC measurement of the photo current map of the top (bottom) cell.

In a second experiment set the blue (IR) laser is modulated with frequency $\omega_a = 2\pi \times 6$ kHz while no background illumination is present and thus no photocurrent is generated in the bottom (top) cell. Thus CM limits the photo current measurements.

In a third experiment set both lasers are modulated with $\omega_a = 2\pi \times 6$ kHz and $\omega_b = 2\pi \times 10$ kHz, respectively, and several maps are recorded simultaneously as discussed in the theory part.

4 RESULTS AND DISCUSSION

4.1 One perturbation frequency

Maps of the first experiment set with one of the two lasers as constant background illumination and one laser modulated with $\omega_a = 2\pi \times 6$ kHz are displayed in Fig. 1. Maps of the second experiment without constant background illumination and one laser modulated with ω_a are displayed in Fig. 2. In Fig. 1a) the constant IR background illumination is "flooding" the bottom cell, i.e. it leads to an excess of photocurrent generated in the bottom cell. Under this condition the current matching condition between top and bottom cell does not limit the photocurrent of the blue laser generated in the top cell. So Fig. 1a) is the conventional LBIC map of the top cell. Correspondingly for Fig. 1c) the top cell is flooded by constant blue laser light, the IR laser photocurrent is not limited by the top cell, and therefore Fig. 1c) is the conventional LBIC map of the bottom cell.

In contrast, in Fig. 2a) the blue laser generated photocurrent in the top cell while there is no photocurrent generated in the bottom cell. So the local dark current, i.e. the leakage current, of the bottom cell is limiting the current through the series connection of the top and bottom cell. Fig. 2a) therefore reflects local properties of the bottom cell which dominate the dark current, e.g. the quality of the p-i-n junction or interface states leading to recombination processes. Analogously Fig. 2c) represents the leakage current of the top cell.

As an example for the additional information which can be extracted from the maps of Fig. 2 the ratio of both

leakage current amplitudes is given in Fig. 4. It surprisingly shows a four-fold symmetry not visible in other maps, which can be explained by non-linear series resistance influences, cf. [3] for a typical series resistance pattern, or by spectral absorption differences of the two lasers. Comparing Fig. 2a) and Fig. 2c) obviously the leakage current distribution of the bottom cell is much more homogeneous than that of the top cell showing a 2-fold symmetry, which is a strong hint that the p-i-n junction of the top cell is degraded at least on the left side.

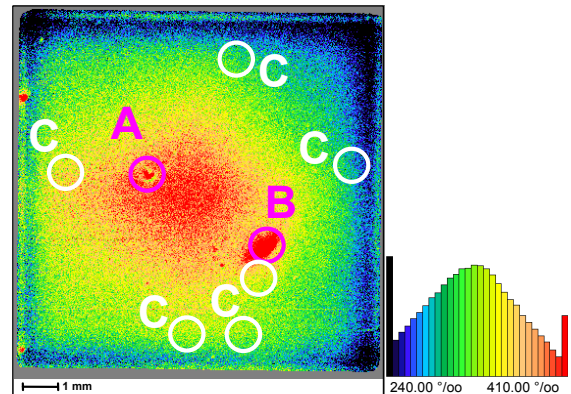


Fig. 4: Blue/IR amplitude ratio of 2nd experiment set, i.e. Fig. 2a) divided by Fig. 2c).

Different local defects denoted as A, B, and C are indicated in Figs. 1–4. In Fig. 2 only two of the localized defects are visible (A and B). The different behavior in the phase shift map of Fig. 2d) already indicates that defects A and B have different reasons. In the ratio map of Fig. 4 defect A is barely visible indicating that A represents a region with increased leakage current in both sub-cells. A possible candidate for such behavior would be a defect at the interface between both sub-cells like a bad tunnel recombination diode leading to increased local recombination in both sub-cells. In contrast, defect B is prominently red in Fig. 4, indicating a region with increased leakage current mainly in the μ -Si bottom cell. A possible explanation might be a worse p-i-n junction. All other defects visible in Fig. 1 highlighted as C are regions with photocurrent losses either in one or both sub-cells that do not appear in the leakage current maps. Thus C defects show only a reduced photocurrent, possibly related to optical losses (high reflectivity), bad generation (thin absorber, ...), or high recombination.

For analyzing LBIC measurements of tandem solar cells a global background illumination is often applied for flooding the adjacent sub-cell. These examples show that local flooding works as well. Photocurrent maps as well as leakage current maps can be measured quite easily. Especially the information about the local leakage current map can be measured even more easily than on standard single junction cells. In the following a second approach will be discussed which allows to extract nearly the same local information within even less measurement time.

4.2 Two perturbation frequencies simultaneously

Fig. 3 presents short-circuit current data measured simultaneously by applying $\omega_a = 2\pi \times 10$ kHz to the blue laser and $\omega_b = 2\pi \times 6$ kHz to the IR laser. Fig. 5 shows an

example for the time dependency of the total photocurrent response. For standard lock-in measurements the asymmetric peaks marked by the black circles would be a strong indication for a measurement error since they can not be explained by linear response. Careful investigation showed that this non-linear response is no measurement artifact but an intrinsic feature of the tandem cell structure. However the non-linear effect according to Eq. (4c) affects the whole period length and is not restricted to these marked regions, thus second-harmonic measurements for the frequencies $2\omega_a$ and $2\omega_b$ (not presented here) and for $\omega_a + \omega_b$ have been used to analyze the second-harmonic generation.

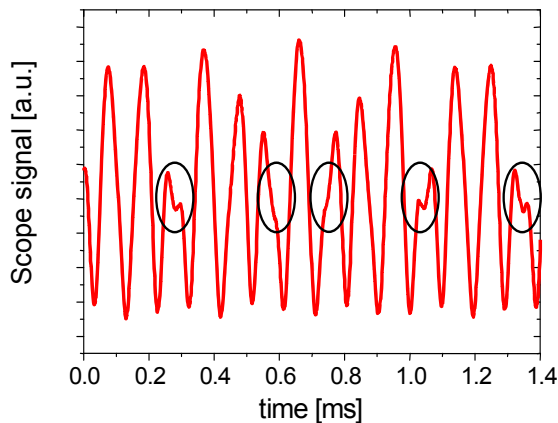


Fig. 5: Multi-frequency response signal of Fig. 3. Black circles mark non-linear behavior that is only visible at certain times.

Fig. 3a) represents the amplitude map of the short-circuit current generated by the blue laser and Fig. 3c) that of the IR laser when both maps are measured simultaneously. Comparison to Fig. 1a) and c) shows nearly identical maps with mean values being only slightly reduced. Despite the fact that none of the sub-cells is flooded with charges in favor of the adjacent cell no significant local current limitations are visible that could be related to missing current matching. This is a quite astonishing result. The ratio between the two blue laser photocurrent maps of Fig. 1a) and Fig. 3a) is shown in Fig. 6. The corresponding map for the IR laser photocurrent is shown in Fig. 7. Despite of a small measurement artifact leading to the horizontal black line in the lower part of Fig. 6, the ratio map is extremely homogeneous; only the area of defect A is visible. The ratio map for the IR laser in Fig. 7 is much more inhomogeneous showing higher losses for Fig. 3c) in the left part than in the right part. There is a clear correlation between Fig. 7 and the leakage current map in Fig. 2c). The same is true for Fig. 6 and Fig. 2a). In summary, for measuring both photocurrent maps simultaneously, current matching seems to be a stronger limiting factor in those regions where the adjacent sub-cell shows low leakage current, i.e. where it has less problems related probably to the p-i-n junction.

Similar results can be extracted from the second-harmonic analysis. Fig. 3e) and f) display the amplitude and phase shift maps for the sum frequency $\omega_a + \omega_b$, their resulting ratio maps according to Eq. (5) are presented in Fig. 3g) and h). Fig. 3g) shows a clear anti-correlation to Fig. 2c). This first of all emphasizes that the second-

harmonic generation in these CELLO measurements really reflects local solar cell properties. It mainly contains the same information as already discussed for Fig. 7: the smallest second-harmonic response is found on the right side of the tandem cell. On this side the IR laser photo current was least influenced by current matching limitation. This is in good agreement with the expectation discussed in the theory part that missing current matching should lead to strong non-linear response.

Up to now the complete discussion only took into account the amplitude maps although the phase shift maps contain valuable independent information. For instance, one phase shift map in Fig. 2d) allows to distinguish between the defect types A and B, instead of at least two amplitude maps needed in contrast. Another important information we can extract from the phase shift map is that the leakage current problems of the top cell are not directly related to local series resistance problems, because no correlation but an anticorrelation is found between the amplitude and phase shift maps in Fig. 2a) and 2b) [1].

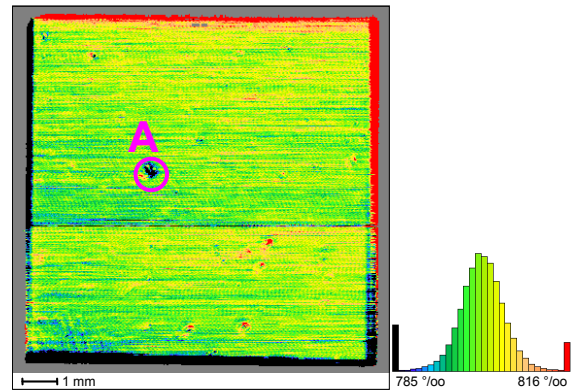


Fig. 6: Blue laser amplitude ratio between third and first measurement set, i.e. Fig. 3a) divided by Fig. 1a).

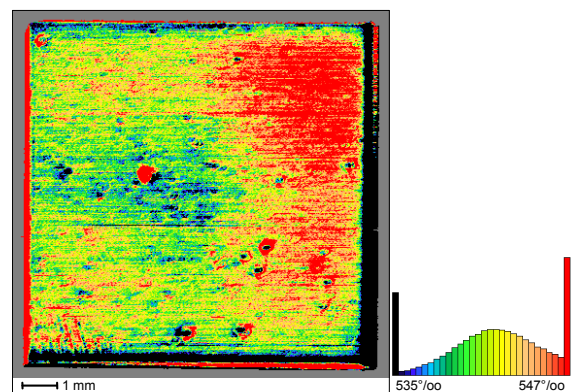


Fig. 7: IR laser amplitude ratio between third and first measurement set, i.e. Fig. 3c) divided by Fig. 1c).

It is not yet clear why Fig. 6 and 7 are very homogeneous (neglecting the leakage current influence in Fig. 7) and the why the mean values for the photocurrent maps measured simultaneously for both sub-cells, Fig. 3a) and c), are so high. Since both sub-cells are in series current matching is needed at any moment. Since both lasers are modulated with different frequencies, a further current source allowing current matching is needed which can not be the leakage current.

All our experimental findings are consistent with the assumption that photo-generated charges which cannot instantly leave one of the sub-cells due to missing current matching may integrate up to some kind of charge depot acting as a current source for satisfying the current matching condition of the adjacent sub-cell. Up to now it is not clear how the depot can be explained in detail. If assuming the depot current is homogeneous and add up to the leakage current, the observed correlation between Fig. 2c) and Fig. 7 and the anti-correlation between Fig. 2c) and Fig. 3g) can be explained.

When starting this kind of analysis we were more astonished to find such a small second harmonic than to find any second harmonic since taking into account only directly generated local photo current and local leakage current, current matching should have a tremendous effect. The charge depot model may be a simple explanation for this discrepancy.

5 CONCLUSION AND OUTLOOK

CELLO measurements of a-Si/ μ -Si tandem cells give consistent results for conventional measurement modes with one scanned laser and various background illuminations and for the new mode with two simultaneously modulated lasers. Additionally, the latter mode is the faster one and allows to extract useful local information about non-linear processes via 2nd harmonic analysis.

For both sub-cells the local leakage current as well as the local photocurrent can be measured allowing to identify various defect types and their location in the p-i-n junctions stack.

The simultaneous photocurrent measurements show that current matching limits much less than expected from simulations. A simple charge depot model has been proposed to explain this. Further measurements especially on tandem solar cells with other concepts, e.g. organic solar cells, are necessary to check if the charge depot is applicable not only to a-Si/ μ -Si cells.

6 ACKNOWLEDGEMENTS

This work was supported by the Deutsche Forschungsgemeinschaft under contract No. FO 285/11-2.

7 REFERENCES

- [1] J. Carstensen, A. Schütt, G. Popkirov, and H. Föll, in Proc. 25th European Photovoltaic Solar Energy Conference, 2CV.3.27, Valencia (2010).
- [2] A. Schütt, J. Carstensen, G. Popkirov, and H. Föll, in Proc. 26th European Photovoltaic Solar Energy Conference, 2DO.3.3, Hamburg (2011).
- [3] M. Nguyen, M. Stegmaier, A. Schütt, J. Carstensen, and H. Föll, in Proc. 27th European Photovoltaic Solar Energy Conference, 3DV.1.59, Frankfurt (2012).